Are your MRI contrast agents cost-effective?
Learn more about generic Gadolinium-Based Contrast Agents.
FRESENIUS KABI
caring for life

AJNR

Curved-Surface Projection: An Alternative Method for Visualizing Functional MR Imaging Results

Lukas Scheef, Klaus Hoenig, Horst Urbach, Hans Schild and Roy Koenig

This information is current as of April 23, 2024.

AJNR Am J Neuroradiol 2003, 24 (6) 1045-1048
http://www.ajnr.org/content/24/6/1045

AJNR Am J Neuroradiol 24:1045–1048, June/July 2003

Curved-Surface Projection: An Alternative Method for Visualizing Functional MR Imaging Results

Lukas Scheef, Klaus Hoenig, Horst Urbach, Hans Schild, and Roy Koenig

Summary: Curved-surface projection (CSP) is a new technique for visualizing functional MR imaging data. This technique helps in identifying anatomic structures by demonstrating the whole gyral and sulcal pattern of the brain at once. Compared with other techniques, CSP preserves the spatial relation of eloquent areas to lesions. Especially in neurosurgical patients with space-occupying lesions, CSP helps in assigning the anatomy to its function.

Functional imaging is becoming more often used for presurgical planning and for guiding neurosurgeons during their interventions. Functional MR imaging (fMRI) can help improve our understanding of the anatomic relationship of a lesion to eloquent areas. This information might be used to optimize resection margins and to reduce the postoperative deficit. However, if a lesion distorts the brain surface or deep anatomy, making the right topographic assignment or understanding the anatomic relation of a lesion to eloquent areas often becomes difficult.

Several approaches are used to display functional imaging results. These include overlaying fMRI results on orthogonally reformatted high-spatial-resolution T1-weighted images, projecting statistical maps onto three-dimensional (3D) models of the rendered brain surfaces, and projecting flat-mounted maps. The first method is most widely used. However, in the case of large space-occupying or deep subcortical lesions, this kind of visualization often fails or requires interactive browsing through all three orthogonal views. Even the more advanced techniques, such as 3D surface rendering and flat mounting, do not solve this problem entirely. We propose an alternative visualization method that has the potential to overcome these difficulties by displaying the gyral pattern as flat maps would do, yet preserve the spatial relationship of the eloquent areas to the lesions.

Description of the Technique

To generate a 3D source dataset, we performed a T1-weighted, high-spatial-resolution, isotropic, 3D gradient-echo pulse sequence on a clinical 1.5-T system (Gyroscan Intera; Philips Medical Systems, Best, the Netherlands) by using a birdcage head coil. The following pulse sequence parameters were used: TR/TE, 12.3/3.6; flip angle, 10°; field of view (FOV), 256 × 256 mm; matrix size, 256; contiguous sections, 150; and section thickness, 1 mm. fMRI was performed with a standard echo-planar imaging sequence, with the following parameters: 3000/50; flip angle, 90°; spatial resolution, 4 × 4 × 4 mm; FOV, 256; matrix size, 64 × 64; and section thickness, 4 mm. The curved-surface projection (CSP) was performed on a standard personal computer (Pentium II processor at 800 MHz, 256 MB RAM) by using a software package developed by two of the authors (R.K., L.S.).

After coregistration of the functional dataset and the anatomic reference dataset by using SPM99 available at *www.fil.ion.ucl.ac.uk/spm* (1), the functional dataset was further preprocessed and analyzed by using the general linear model as implemented in SPM99. The thresholded statistical map ($P < .05$, corrected) was written into a separate file and interpolated to fit the spatial resolution of the structural reference dataset. The interpolated map was then superimposed on the reference dataset by using the image calculation option of SPM99.

Our approach to visualizing the fMRI results was to reconstruct the fused dataset on curved planes parallel to the brain surface. We called this visualization method CSP.

The first step in performing CSP was the definition of a path parallel to the brain surface on a coronal view of the 3D-volume dataset (Fig. 1). The (curved) surface is constructed by parallel shifting of the defined path in an anteroposterior direction (Fig 2). By collapsing the path in the direction of the surface gradients with the normal evolution algorithm described by Gomes et al (2), (Fig 1), the whole brain can be automatically reformatted, and therefore, structures in any depth become accessible. The resulting planes are unfolded by using a Mercator projection (3), (Fig 3). If the functional maps are not fused with the anatomic reference image at the beginning, this can be performed at the final stage by applying the transformation matrix onto the statistical map.

Discussion

The projection of thresholded statistical maps on high-spatial-resolution 3D datasets is commonly used to visualize fMRI results. Results can be analyzed either by browsing orthogonal projections of the statistical maps or by viewing the projections on 3D-rendered brain surfaces. After normalization of the data into the Talairach (4) or Montreal Neurological Institute space (5) the coordinates can additionally be used to locate focal brain activity (6). A more advanced technique is the projection of activity maps onto inflated and flat-mounted brains to visualize the two-dimensional topology of the cerebral cortex (7, 8).

However valuable these techniques may be for analyzing volunteer data, they tend to fail if a lesion

Received August 23, 2002; accepted after revision, December 9.

From the Department of Radiology, University of Bonn, Germany.

Address reprint requests to Lukas Scheef, MD, MSc, Department of Radiology, University of Bonn, Sigmund-Freud-Straβe 25, D-53105 Bonn.

© American Society of Neuroradiology

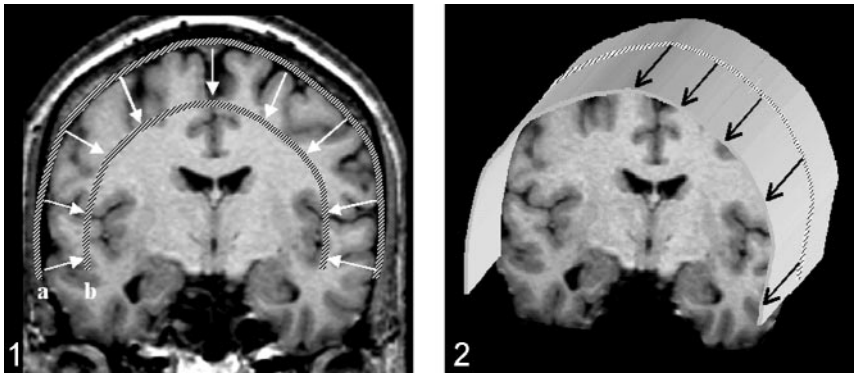

FIG 1. Definition of a path along the outer curvature of the brain. After the first path is defined, additional paths can be calculated by collapsing the initial path parallel to the path gradients. Displayed are the outer (*a*) and the inner (*b*) paths, which define the reconstructed volume. The thickness of the slab to be reconstructed as curved surfaces, as well as the section thickness, can be freely chosen.

FIG 2. Construction of a curved surface by means of parallel shifting of a predefined path.

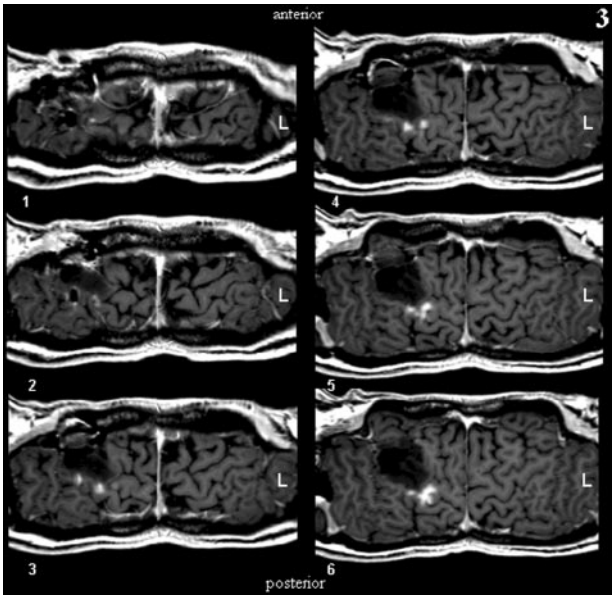

FIG 3. The first six reconstructed sections defined in Figure 1 are displayed (section thickness, 1 mm).

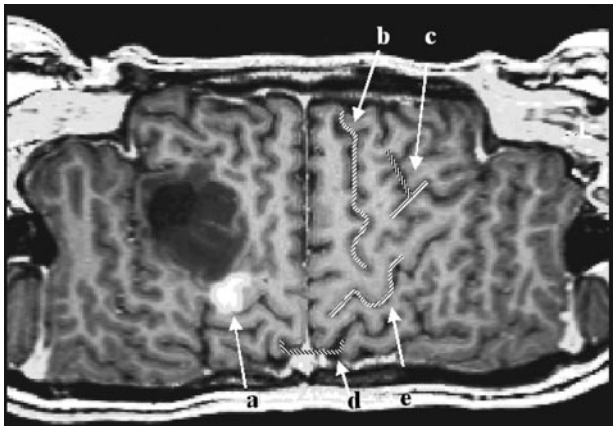

FIG 4. Figure shows the result of an finger-tapping experiment on a T1-weighted reference image (block design, self-paced finger tapping of the left hand). The examination was performed in the context of presurgical evaluation of a patient after recurrence of a frontocentral astrocytoma (World Health Organization grade III) in the right hemisphere. The tumor margins reach the precentral gyrus close to the hand area of the primary motor cortex. The motor area, as detected with fMRI, is marked in *white* (*a*). The central sulcus can be identified by using five anatomic features: *1*, The superior frontal sulcus ends in the precentral gyrus (*b*). *2*, The lower part of the precentral sulcus and the inferior sulcus define the T sign (*c*). *3*, The bracket sign defines the interception of the marginal part of the cingulate sulcus and the central sulcus close to the midline (*d*). *4*, The omega shape of the precentral gyrus defines the hand motor area, the hand knob of the primary motor cortex (*e*). *5*, The relative thickness of the precentral gyrus to the postcentral gyrus (pre > post) can help in identifying the central sulcus (*e*)

distorts the brain, and browsing 3D datasets can become a tedious and time-consuming job. The anatomic-functional assignment often fails, because the standard technique does not provide a survey of the gyral and sulcal pattern. In particular, the identification of the central sulcus is often problematic because of its oblique progression from a posterior-medial to an anterior-lateral inferior direction. To find the central sulcus, the datasets have to be viewed section by section. Viewing both hemispheres in all three planes simultaneously could help in this situation, but most programs lack this feature. However, even if both hemispheres can be displayed and browsed simultaneously in three orthogonal planes, following the sulcal or gyral patterns on those images is still error prone.

Identifying structures on 3D-rendered surfaces often becomes difficult when lesions and their surrounding edema blur the gyral and sulcal patterns. Additionally, in considering subcortical lesions, this method does not provide any information about the relation of a lesion to eloquent brain areas. Furthermore, Talairach coordinates are not precise enough in labeling anatomic structures, and they are invalid and must not be used when space-occupying lesions distort the regular anatomy. Even with more advanced techniques, such as inflating and flat mounting as performed by FreeSurfer available at *surfer.nmr.mgh.harvard.edu* (7, 8), the problem is not entirely solved. Flat-mounted maps reveal the entire gyral and sulcal pattern at once and help in identifying anatomic structures, yet they lose the topographic relation between anatomy and function in cases of subcortical lesions. The reason for this limitation is that the gray matter–white matter segmentation needed for constructing inflated and flat-mounted surfaces can be flawed if lesions are present. This error occurs because segmentation often depends on prior information such as gray matter–white matter probability maps, which are only conditionally applicable in patients with lesions, brain atrophy, and so forth. In addition, lesions are likely to change the topology of

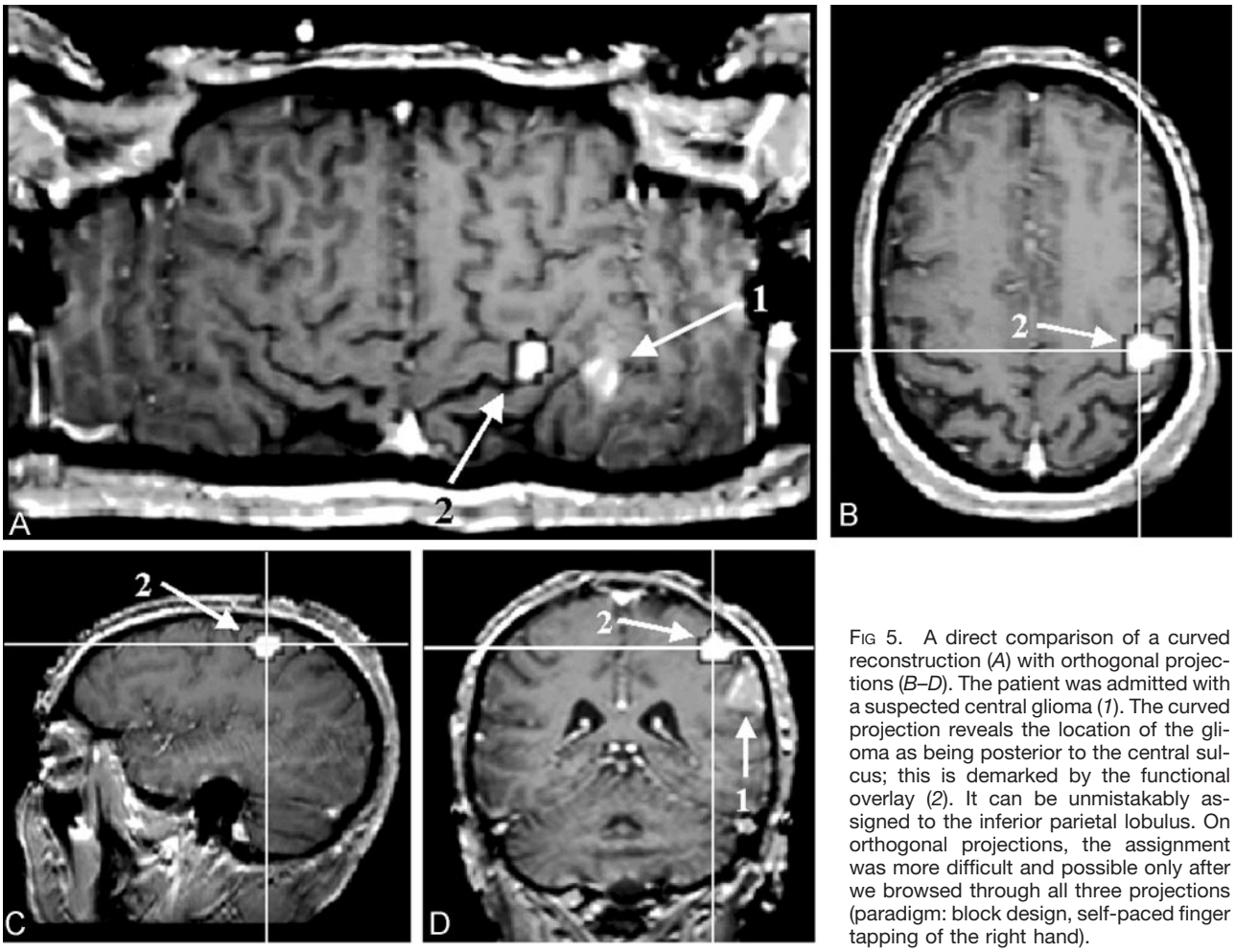

FIG 5. A direct comparison of a curved reconstruction (*A*) with orthogonal projections (*B–D*). The patient was admitted with a suspected central glioma (*1*). The curved projection reveals the location of the glioma as being posterior to the central sulcus; this is demarked by the functional overlay (*2*). It can be unmistakably assigned to the inferior parietal lobulus. On orthogonal projections, the assignment was more difficult and possible only after we browsed through all three projections (paradigm: block design, self-paced finger tapping of the right hand).

the brain by adding holes into the segmentation maps, which may result in difficulties or failure of the inflating algorithm. In addition, inflating and flat mounting are time-consuming techniques. Depending on the software used, 12–24 hours are required to transform and reconstruct one hemisphere on a modern personal computer. Therefore, this approach is not suitable for use in a clinical setting.

As opposed to the previously mentioned visualization methods, CSP displays the gyral and sulcal patterns of both hemispheres at the same time, enabling a direct side-to-side comparison of the gyral and sulcal patterns. This capability is exceedingly helpful for the identification of the exact sulcal and gyral topography of a space-occupying lesion. Because CSP does not rely on any assumption as the topologic structure of the anatomic reference dataset or on a segmentation process, deteriorated tissue contrast that goes along with cortical and subcortical lesions does not impair the accuracy of the results. With CSP, a multitude of anatomic landmarks, such as the bracket sign, the T sign, the Omega-sign, and so forth (9–10) (see Fig 4), can be visualized simultaneously. Therefore, even if a lesion destroys one or several landmarks, enough anatomic features should still be left to enable a direct topographic assignment. The orientation is consequently less time consuming as compared with the anatomic analysis of orthogonally reformatted datasets (11), (Fig 5).

Nevertheless, we should mention at this point that the method just described helps in visualizing fMRI results, but it does not overcome the problem of potential misregistration between anatomic and functional datasets owing to the well-known artifacts of echo-planar imaging. These must especially be kept in mind when fMRI is used in a clinical setting.

From a practical point of view, an additional advantage of the curved reconstruction is its simplicity. The computational power needed is far less than that needed for flat-mounting techniques. Even on a low-budget computer, the reconstruction of the surfaces can be performed almost in real time; this ability makes the method suitable for daily, routine clinical use, without adding extra time or cost. The simplicity of the algorithm also allows us to incorporate information gained by using other techniques, such as electrophysiologic data, as provided by subdural electrode grids (12).

Curved-surface reconstructions can also aid in teaching brain anatomy by offering better visualization of the gyral and sulcal topology. By reformatting high-spatial-resolution T1-weighted images on curved planes, the anatomic connectivity between sulci and gyri becomes easily accessible. Different anatomic land-

marks and their anatomic relation to each other can be visualized on one section. Therefore, this method can help in obtaining a better understanding of the anatomic relationship of cortical structures. Having internalized these relationships, one may find it easier to orient them on standard pathology sections.

Conclusion

CSP is a helpful, time-saving, and cost-effective method to display the spatial relationships among functions, lesions, and anatomy of the brain. The biggest advantage of CSP, compared with existing methods, is its ability to show the gyral and sulcal patterns of both hemispheres at the same time, simplifying their orientation on the reconstructed maps. Because this technique does not rely on any segmentation process or any assumption of the topologic structure of the anatomic reference dataset, CSP can be applied, even if the brain anatomy is largely distorted. The robustness and simplicity of the algorithm make CSP ideally suited for the clinical daily use in the presurgical planning and analysis of brain function.

References

1. Friston K, Holmes AP, Worsely KJ, Poline JB, Frith CD, Franckowiak RSJ. **Statistical parametric maps in functional imaging: a general linear approach.** *Human Brain Mapping* 1995;2:189–210
2. Gomes J, Darsa L, Costa B, Velho L. *Warping and Morphing of Graphical Objects.* San Francisco: Morgan Kaufmann Publishers, Inc. 1999;326–329
3. Sachs JM. **A curious mixture of maps, dates, and names.** *Mathematics Magazine* 1987;60:151–158
4. Talairach J, Tournoux P. **Co-planar stereotaxic atlas of the human brain.** New York: Thieme; 1988
5. Evans AC, Collins DL, Mills SR, Brown ED, Kelly RL, Peters TM. **3D statistical neuroanatomical models from 305 MRI volumes.** *Proceedings of the IEEE-Nuclear Science Symposium and Medical Imaging Conference*. Chicago, IEEE; 1993
6. Lancaster JL, Woldorff MG, Parsons LM, et al. **Automated Talairach atlas labels for functional brain mapping.** *Hum Brain Mapp* 2000;10:120–131
7. Dale AM, Fischl B, Sereno MI. **Cortical surface-based analysis, I: segmentation and surface reconstruction.** *NeuroImage* 1999;9:179–194
8. Fischl B, Sereno MI, Dale AM. **Cortical surface-based analysis, II: inflation, flattening, and a surface-based coordinate system.** *NeuroImage* 1999;9:195–207
9. Naidich TP, Brightbill TC. **Systems for localizing fronto-parietal gyri and sulci on axial CT and MRI.** *Int J Neuroradiology* 1996;2:313–338
10. Naidich TP, Valavanis AG, Kubik S. **Anatomic relationships along the low-middle convexity: normal specimens and MRI.** *Neurosurgery* 1995;36:517–532
11. Braks E, Hattingen J, Clussmann H, Meyer B, Urbach H, Schild H. **Die Hirnoberfläche als "Landkarte"- eine hilfreiche Ansicht zur Lokalisation zerebraler Läsionen? 81.** Deutscher Röntgenkongress; May 31–June 3, 2000; Wiesbaden, Germany
12. Koenig R, Urbach H, Oertzen J von, et al. **Entwicklung eines neuen Algorithmus zur Projektion von Gitterelektroden auf planare Hirnoberflächenprojektionen (sog. Pancake-Reformatierung). 83.** Deutscher Röntgenkongress; May 8–11, 2002; Wiesbaden, Germany

In Re: Characterization of Benign and Metastatic Vertebral Compression Fractures with Quantitative Diffusion MR Imaging

We enjoyed reading the recent article by Zhou et al (1) on the application of quantitative diffusion imaging to the differential diagnosis of benign versus metastatic vertebral compression fractures. This article and the accompanying editorial provided useful insights into both the clinical dilemma posed by this problem and the limitations of current MR imaging methodology in addressing it. As we see it, the major "talking point" from the article is that quantitative diffusion imaging improves upon the use of qualitative diffusion-weighted imaging by eliminating the confounding effects of "T2 shine-through." Although this improvement on the use of diffusion-weighted imaging alone is appreciated, it is our concern that the article under consideration and the few previous works in this arena (2–4) have either ignored or failed to appreciate adequately the extent to which lipid signal intensity within vertebral marrow may contribute to quantitative measurements of the tissue diffusion coefficient. Indeed, the discussions in these articles regarding the differences between diffusion characteristics of benign versus metastatic vertebral compression fractures tend to focus on the same biophysical mechanisms used to describe diffusion characteristics in brain and brain abnormalities where, of course, any lipid component can be safely ignored. This is not so in vertebral marrow; we demonstrate in this letter how even a fairly small fraction of lipid within a voxel can drastically affect diffusion coefficient measurements.

Healthy vertebral marrow contains some 20–70% lipid (5–12) with, according to the early spectroscopic studies of De Bisschop et al (5), approximately 7% increase in fat percentage per decade of life. Thus, a voxel of healthy vertebral marrow will contain a substantial signal intensity component from lipid. With the infiltration of malignant tumor or a more benign edematous process, the lipid component of the proton signal intensity can be expected to diminish. In our opinion, however, complete replacement of the lipid component with water will represent only an extreme condition. Thus, the tendency to ignore the lipid contribution—for either qualitative interpretations of diffusion-weighted imaging (2–4) or quantitative tissue diffusion measurements (1) within vertebral marrow, particularly when fat saturation or selective water excitation is not included in the pulse sequence design (1–4)—is simply not appropriate.

To justify this opinion requires consideration of how the lipid signal intensity can be anticipated to affect quantitative tissue diffusion coefficient measurements in vertebral marrow. Here we rely on our own measurements of the lipid diffusion coefficient in human scalp in vivo, which revealed that the large, slowly diffusing triglyceride molecules have a low diffusion coefficient D_f, of approximately 0.05 $\mu m^2/ms$ (13). Let us now assume for the sake of argument that the water tissue diffusion coefficient D_w, takes a value of 1.9 $\mu m^2/ms$ as reported by Zhou et al for metastatic fractures within vertebral marrow (1). Because water and lipid protons do not exchange, the overall decay of signal intensity with b factor will then be described by a biexponential function of the form

$$S = W\exp(-bD_w) + F\exp(-bD_f), \quad 1)$$

where W and F are the apparent amplitudes of the water and fat protons, respectively. The term "apparent" is used, because W and F do not represent solely the respective water and fat proton densities, but also T1 and T2 weightings. These in turn depend on the specifics of the pulse sequence (echo and repetition times) in combination with the fat and water relaxation times for which there is an established literature (9–12). Letting $F + W = 1$ for normalization purposes, simulations based on equation 1 were generated for both an extended b factor range up to 3000 s/mm^2 and for the more limited range below 300 s/mm^2 employed by Zhou et al and others to study diffusion in vertebral marrow (1–4). Semilog plots of S versus b factor are provided in Figure 1, where the different curves in each plot represent different fat fractions from 0.05 (+), 0.15 (0), 0.25 (*),and 0.35 (−). Over the extended b factor range (top plot) the nonmonoexponential nature of equation 1 reveals itself quite clearly as a curvature over the extended b factor range. Over the more limited b factor range relevant to the current clinical studies (lower plot), the decays actually appear monoexponential, but with lower diffusion coefficients (smaller slopes) observed with increasing fat fraction. Closer analysis of the simulated slopes reveals a nearly linear decrease with fat fraction in the apparent diffusion coefficient D_{app}, in this low b factor range. Figure 2 shows how a "monoexponential"-based D_{app} would be measured by using four b factors of 5, 70, 135, and 200 s/mm^2 as the fat fraction increases from 0.05

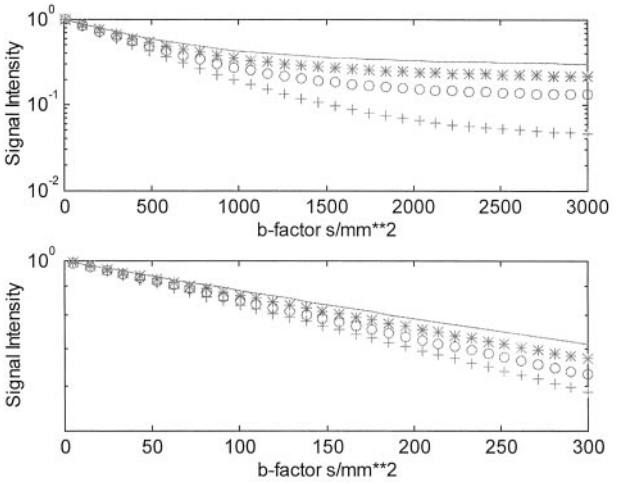

FIG 1. Simulated semilog plots of signal intensity versus b factor for marrow with varying fractions of fat for extended b factor range (*top plots*) and the limited b factor range used to date in most studies of vertebral marrow.

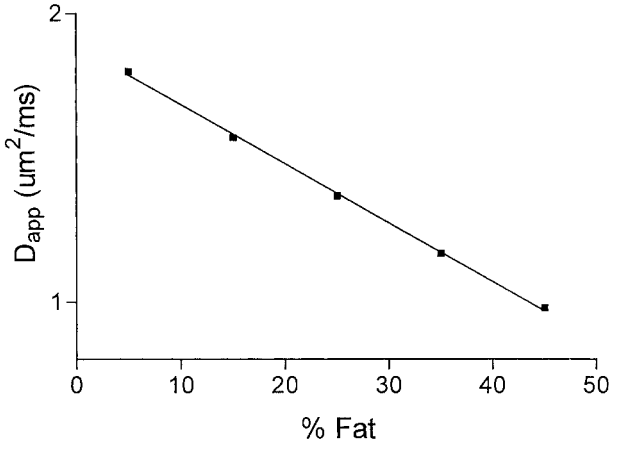

FIG 2. Plot of the apparent diffusion coefficient as a function of fat fraction in vertebral marrow when measured over the limited b factor range from 0 to 200 s/mm^2.

to 0.45. The correlation coefficients r^2 for the linear regressions of the ln(S) versus b factor fits used to obtain the D_{app} values were all above 0.999, effectively disguising the biexponential nature of the signal intensity decay due to the lipid component in this b factor range. Rather, the primary effect of increasing fat fraction in this low b factor range is to "artificially" lower D_{app}. The simulated results of Figure 2 are well represented by a linear regression fit as

$$D_{app} = 1.88 - 0.02F, \quad (2)$$

with an $r^2 > 0.99$.

To conclude, we were concerned that Zhou et al and others who have begun to explore the potential of diffusion imaging in vertebral marrow have paid too little attention to the consequences of a lipid component on diffusion-weighted images and quantitative diffusion measurements. Figure 2 demonstrates how even small percentages of lipid within a voxel can dramatically affect the measured value of the diffusion coefficient. Because the non-echo-planar–based pulse sequences used to date for the vertebral marrow studies have not employed water selective or fat suppression methods (1–4), many of the forwarded interpretations of diffusion characteristics based on water specific models common to brain discussions seem premature.

Robert V. Mulkern
Richard B. Schwartz
Department of Radiology
Children's Hospital and Brigham and Women's Hospital
Harvard Medical School
Boston, Massachusetts

References

1. Zhou XJ, Leeds NE, McKinnon GC, Kumar AJ. **Characterization of benign and metastatic vertebral compression fractures with quantitative diffusion MR imaging.** *AJNR Am J Neuroradiol* 2002; 23:165–170
2. Baur A, Stabler A, Bruning R, et al. **Diffusion-weighted MR imaging of bone marrow: differentiation of benign versus pathologic compression fractures.** *Radiology* 1998;207:349–356
3. Le Bihan DJ. **Differentiation of benign versus pathologic compression fractures with diffusion-weighted MR imaging: a closer step toward the "holy grail" of tissue characterization?** *Radiology* 1998; 207:305–307
4. Castillo M, Arbelaez A, Smith JK, Fisher LL. **Diffusion-weighted MR imaging offers no advantage over routine noncontrast MR imaging in the detection of vertebral metastases.** *AJNR Am J Neuroradiol* 2000;21:948–953
5. De Bisschop E, Luypaert R, Louis O, Osteuax M. **Fat fraction of lumbar bone marrow using in vivo proton nuclear magnetic resonance spectroscopy.** *Bone* 1993;14:133–136
6. Mulkern RV, Meng J, Oshio K, et al. **Bone marrow characterization in the lumbar spine with inner volume spectroscopic CPMG imaging studies.** *J Magn Reson Imaging* 1994;4:585–589
7. Schellinger D, Lin CS, Fertikh D, et al. **Normal lumbar vertebrae: anatomic, age, and sex variance in subjects at proton MR spectroscopy—initial experience.** *Radiology* 2000;215:910–916
8. Jung CM, Kugel H, Schulte O, Heindel W. **Proton-MR-spectroscopy of vertebral bone marrow: normal age- and sex-related patterns.** *Radiologue* 2000;40:694–699
9. Kugel H, Jung C, Schulte O, Heindel W. **Age- and sex-specific differences in the 1H-spectrum of vertebral bone marrow.** *J Magn Reson Imaging* 2001;13:263–268
10. Traber F, Block W, Layer G, et al. **Determination of 1H relaxation times of water in human bone marrow by fat-suppressed turbo spin echo in comparison to MR spectroscopic methods.** *J Magn Reson Imaging* 1996;6:541–548
11. Masumoto A, Yonekura S, Haida M, et al. **Analysis of intramedullary cell density by MRI using the multiple spin-echo technique.** *Am J Hematol* 1997;55:134–138
12. Schick F, Bongers H, Jung WI, et al. **Proton relaxation times in human red bone marrow by volume selective magnetic resonance spectroscopy.** *Appl Magn Reson* 1992;3:947–963
13. Mulkern RV, Gudbjartsson H, Westin C-F, et al. **Multi-component apparent diffusion coefficients in human brain.** *NMR Biomed* 1999; 12:51–62

Reply:

We thank Drs. Mulkern and Schwartz for their careful review of our article (1) and appreciate the opportunity to respond to their comments.

Drs. Mulkern and Schwartz expressed concern that our article, as well as several others on the same subject (2, 3), did not discuss the influence of lipid signal on diffusion-weighted images and on measurement of apparent diffusion coefficient (ADC) of vertebral bodies. On the basis of a two-compartment model that accounts for water and fat, they presented an empirical relationship between the ADC and the lipid fraction F (see Equation 2 of Drs. Mulkern and Schwartz's letter). This relationship indicates that the presence of lipid signal can contaminate the results in quantitative diffusion analysis, an aspect we did not consider in our article.

In *healthy* vertebral marrow, lipid content can be as high as 70% (4). Therefore, it is not negligible. For the two diseases we studied, however, the lipid fraction in the vertebral marrow can be considerably less. According to a study by Yuh et al (5), approximately 88% of vertebral metastasis cases exhibited *total* replacement of normal bone marrow. Similarly, edema in benign vertebral compression fractures can also replace normal marrow, resulting in substantially decreased lipid content in the lesion (6). In our study, the ADC values were calculated within a region of interest that contained *only* the vertebral lesion. Within the region of interest, the signal intensity of diffusion-weighted images arises predominantly from water, as evidenced by the T1-weighted, T2-weighted, and postcontrast T1-weighted images with or without fat suppression (Figs 1 and 2 in our article [1]). Therefore, we think it is appropriate to qualitatively discuss our results by using a water-only model.

Quantitatively, lipid signals within the region of interest can arise from either incomplete bone marrow replacement or the partial volume contamination. Thus, we agree with Drs. Mulkern and Schwartz that the possible presence of lipid should be considered. If we assume that the lipid fraction ranges from 0% to 20% among the regions of interest of the metastatic lesions in our study, equation 2 of Drs. Mulkern and Schwartz's letter indicates that the ADC value would vary between 1.88 and 1.48 mm^2/s, with a standard deviation of 0.2 mm^2/s. This standard deviation is not larger than what we observed in the study and is already contained in the error term (± 0.3 mm^2/s) we reported.

For normal vertebral bodies, wherein the lipid content cannot be neglected, we completely agree with Drs. Mulkern and Schwartz that a two-compartment model should be used to characterize the signals in diffusion-weighted images and determine the ADC values for water and fat separately. The primary focus for our article, however, was to present a possible way to differentiate benign from malignant vertebral compression fractures, not to provide a detailed account of the diffusion process in normal vertebral bodies.

In summary, Drs. Mulkern and Schwartz raised an important question in analyzing diffusion-weighted images and interpreting the ADC values in regions wherein both water and lipid signals are present. Within benign and malignant vertebral compression fractures, the impact of the lipid signal intensity is minimal. Thus, our explanation based on water diffusion remains valid and our conclusions unchanged. To extend quantitative diffusion imaging to other vertebral lesions, such as hemangiomas, we recommend that fat suppression techniques (eg, by using chemical suppression or spatial spectral excitation

radio-frequency pulses) be employed to reduce the effect of lipid signal intensity on ADC quantification.

Xiaohong Joe Zhou, Normal E. Leeds, and Ashok J. Kumar
M. D. Anderson Cancer Center
Houston, Texas
Graeme C. McKinnon
Applied Science Laboratory
General Electric Medical Systems
Milwaukee, Wisconsin

References

1. Zhou XJ, Leeds NE, McKinnon GC, Kumar AJ. **Characterization of benign and metastatic vertebral compression fractures with quantitative diffusion MR imaging.** *AJNR Am J Neuroradiol* 2002; 23:165–170
2. Baur A, Stabler A, Bruning R, et al. **Diffusion-weighted MR imaging of bone marrow: differentiation of benign versus pathologic compression fractures.** *Radiology* 1998;207:349–356
3. Castillo M, Arbelaez A, Smith JK, Fisher LL. **Diffusion-weighted MR imaging offers no advantage over routine non-contrast MR imaging in the detection of vertebral metastases.** *AJNR Am J Neuroradiol* 2000;21:948–953
4. Kuchel PW, Coy A, Stilbs P. **NMR "diffusion-diffraction" of water revealing alignment of erythrocytes in a magnetic field and their dimensions and membrane transport characteristics.** *Magn Reson Med* 1997;37:637–643
5. Yuh WTC, Zachar CK, Barloon TJ, et al. **Vertebral compression fractures: distinction between benign and malignant cause with MR imaging.** *Radiology* 1989;172:215–218
6. Lafforgue P, Bayle O, Massonnat I, et al. **Magnetic-resonance-imaging of osteoporotic and metastatic vertebral compression fractures in 60 patients.** *Ann Radiol (Paris)* 1991;34:157–166

Subtraction Helical CT Angiography of Intra- and Extracranial Vessels: Technical Considerations and Preliminary Experience—Rediscovery of Matched Mask Bone Elimination?

We read with interest the article on subtraction angiography of the intra- and extracranial vessels by Jayakrishnan et al (1) in the March 2003 issue of the *AJNR*. From the authors' description, we surmise that their technique is a variant of a technique we have routinely used in our hospital for more than 4 years.

We would like to make the following comments. As in all subtraction techniques, two scans are made: one precontrast and the other postcontrast. We understand, however, that the first scan is used to identify the high attenuation structures (ie, bones and calcifications) and that this information is used to mask these structures in the postcontrast scan. If this assumption is correct, the term "subtraction" for this procedure is understandable—actually we used the same phrase in our first communication on this subject (2)—but it is incorrect. In subtraction, all the pixels in the volume of interest are involved, which leads to an overall deterioration of the image quality because of the increase of image noise, whereas in masking only the CT values of the high attenuation pixels are affected. This difference is especially important when the precontrast scan is made with a low dose. In an article on this subject (3), we explained this last method (matched mask bone elimination, or MMBE) and clearly demonstrated the advantages of masking over subtraction.

The use of a vacuum-type head holder to minimize movement is an interesting addition to this technique. The authors state that the use of this head holder *facilitates* image registration. From the information given in the rest of this article, we assume, however, that no registration is performed at all. In our experience, even the slightest movement of the patient in between the scans (in the order of 0.05 mm) may lead to a serious degradation in image quality. If (as we assume) the authors do not use any registration, it would be interesting to investigate whether addition of such a registration step would produce an improvement in the quality of the processed images.

The use of image registration is completely feasible in a routine clinical setting. The authors give a mean postprocessing time for their procedure of slightly more than 8 minutes, by using software of the Omipro workstation of the CT-Twin CT-scanner. For comparison, the processing time of the MMBE software initially was in the order of 1 hour for one examination (3); because of improvements of the software and better performance of the hardware, this time has now been reduced to less that 10 minutes.

Hank W. Venema
Department of Radiology and
Medical Physics
Gerard J. den Heeten
Department of Radiology
University of Amsterdam
Amsterdam, the Netherlands

References

1. Jayakrishnan VK, White PM, Aitken D, et al. **Subtraction helical CT angiography of intra- and extracranial vessels: technical considerations and preliminary experience.** *AJNR Am J Neuroradiol* 2003; 24:451–455
2. Venema HW, Hulsmans FJH, Van Lienden KP, den Heeten GJ. **CT angiography with 0.5 mm collimation of the circle of Willis and the intracranial part of the internal carotid arteries: maximum intensity projection (MIP) with matched mask subtraction.** *Radiology* 1999; 213(P):311
3. Venema HW, Hulsmans FJH, den Heeten GJ. **CT angiography of the circle of Willis and intracranial internal carotid arteries: maximum intensity projection with matched mask bone elimination—feasibility study.** *Radiology* 2001;218:893–898

Reply:

We would like to thank Drs. Venema and den Heeten for their comments on our article (1).

We used the term "subtraction" in a manner consistent with the terminology used in the Omnipro workstation to describe the process of subtracting a 3D mask from the 3D maximum intensity projection image. This does not mean a pixel-by-pixel subtraction, which will of course result in increased noise.

We did not use any image registration protocol in this study, because we often scan the head and neck and the degree of movement generated are probably more than what can be handled by such registration methods. It is for this reason we highlighted the use of the vacuum bag, which is a very good method of immobilization and is well tolerated by the patients. We agree with the Drs. Venema and den Heeten in that even the slightest movement between the scans can seriously degrade the image quality. To counter this, a further process of 3D mask expansion was sometimes employed, usually a one-pixel expansion was sufficient to reduce the artifacts to an acceptable level—a process similar to that used by Venema et al. (2).

V. K. Jayakrishnan
Department of Neuroradiology
The James Cook University Hospital
Middlesbrough
United Kingdom

References

1. Jayakrishnan VK, White PM, Aitken D, et al. **Subtraction helical CT angiography of intra and extracranial vessels: technical considerations and preliminary experience**. *AJNR Am J Neuroradiol* 2003; 24:451–455
2. Venema HW, Hulsmans FJH, den Heeten GJ. **CT angiography of the circle of Willis and intracranial internal carotid arteries: max-**

imum intensity projection with matched mask bone elimination—feasibility study. *Radiology* 2001;218:893–898

Aortic Arch Origin of the Left External Carotid Artery

We read with interest the article by Horowitz et al (1) in the March 2003 issue of the *AJNR*. The authors described an aortic arch origin of the left external carotid artery associated with a type II preatlantal fetal anastomosis. They claim that their case is unique, because it shows a left external carotid artery originating from the aortic arch.

We would like to draw the authors' attention to the previously published reports of left external carotid arteries that have separate origins from the aortic arch. A search of the literature starting from 1968 revealed five cases of agenesis of left common carotid artery with separate origins of the left internal and external carotid arteries from the aortic arch. The condition was diagnosed by MR angiography of supraaortic vessels in a case by Cakirer et al (2), by using a combination of intraarterial angiography and duplex sonography in a case by Woodruff et al (3), and by using intraarterial angiography in three other cases by Bryan et al (4), Dahn et al (5), Rossitti et al (6).

The authors also claim that their case is unique in its association with a type II proatlantal intersegmental artery. Lie (7) reported that there were many congenital anomalies associated with separate origins of left internal and external carotid arteries from the aortic arch, including a cervical aortic arch, a double aortic arch, persistent trigeminal artery, and persistent proatlantal segmental artery in an angiographic study and review of congenital anomalies of the carotid arteries.

Sinan Cakirer and Ercan Karaarslan
Istanbul Sisli Etfal Hospital

References

1. Horowitz M, Bansal S, Dastur K. **Aortic arch origin of the left external carotid artery and type II proatlantal fetal anastomosis.** *AJNR Am J Neuroradiol* 2003;24:323–325
2. Cakirer S, Karaarslan E, Kayabali M, Rozanes I. **Separate origins of the left internal and external carotid arteries from the aortic arch: MRA findings.** *AJNR Am J Neuroradiol* 2002;23:1600–1602
3. Woodruff WW III, Strunsky VP, Brown NJ. **Separate origins of the left internal and external carotid arteries directly from the aortic arch: duplex sonographic findings.** *J Ultrasound Med* 1995;14:867–869
4. Bryan RN, Drewyer RG, Gee W. **Separate origins of the left internal and external carotid arteries from the aorta.** *AJR Am J Roentgenol* 1978;130:362–365
5. Dahn MS, Kaurich JD, Brown FR. **Independent origins of the internal and external carotid arteries: a case report.** *Angiology* 1999; 50:755–760
6. Rossitti S, Raininko R. **Absence of the common carotid artery in a patient with a persistent trigeminal artery variant.** *Clin Radiol* 2001;56:79–81
7. Lie TA. *Congenital anomalies of the carotid arteries: an angiographic study and a review of the literature.* Amsterdam: Excerpta Medica Foundation; 1968;30–35

Reply:

We greatly appreciate the information provided by Drs. Cakirer and Karaarslan regarding prior reports on aortic arch origins of the external carotid artery along with their association with proatlantal vessels. We apologize for incomplete review of the past literature. Once again, we have had it reinforced in our minds that there is rarely "something new under the sun." In retrospect, perhaps I should mind the valuable advice given to me by my mentor, Dr. Philip Purdy, several years ago, when he urged me never to say something is being reported for the first time, because one can be sure that this is not true.

Michael Horowitz
University of Pittsburgh

Diagnosis of Pseudosubarachnoid Hemorrhage

The recently published description of CT findings in pseudosubarachnoid hemorrhage (1) has, unfortunately, omitted to include neuropathologic correlation, despite the authors noting that subarachnoid hemorrhage was excluded on the basis of autopsy in three of the seven cases described. Despite this, the authors suggested that one possible cause for their findings—increased attenuation in the basal cisterns—was superficial vascular engorgement and dilatation (1). If this were true, enhancement following the administration of intravenous contrast medium could prove to be a useful method for confirming this diagnosis, as occurred in one of their cases. In, to my knowledge, the largest published series with this condition with detailed neuropathologic correlation (2), all five cases demonstrated increased attenuation in the basal cisterns, with (at autopsy) histologic evidence of congested and dilated subarachnoid and pial vessels in each, in addition to cerebral edema. Although Given and colleagues may be excused for omitting the latter article in their comprehensive literature review as the journal in which it was published was not—at that time—indexed by Medline, it indicates that the main cause for the CT appearances is vascular engorgement. Future studies should be directed toward determining whether head CT following the administration of intravenous contrast medium is a means of confirming this diagnosis when it is suspected clinically.

Morry Silberstein
School of Medicine
Monash University
Melbourne, Australia

References

1. Given CA, Burdette JH, Elster DA, Williams DW. **Pseudo-subarachnoid hemorrhage: a potential pitfall associated with diffuse cerebral edema**. *AJNR Am J Neuroradiol* 2003;24:254–256
2. Opeskin K, Silberstein M. **False-positive diagnosis of subarachnoid haemorrhage on computed tomography scan.** *J Clin Neurosci* 1998; 5:382–386

Reply:

As discussed in our publication (1), one of the contributing causes for the pseudosubarachnoid hemorrhage appearance seen with diffuse cerebral edema in engorgement of the superficial (pial) vasculature. We would like to thank Dr. Silberstein for bringing to our attention the publication by Operskin and Silberstein (2), because it provides further support for vascular engorgement being a contributing factor in pseudosubarachnoid hemorrhage appearance. Contrasted studies may demonstrate enhancement of the subarachnoid space in such cases and prove useful for further evaluation in when the diagnosis is suspected.

Curtis A. Given II
University of Kentucky Chandler Medical Center
Lexington, Kentucky

References

1. Given CA, Burdette JH, Elster DA, Williams DW. **Pseudo-subarachnoid hemorrhage: a potential pitfall associated with diffuse cerebral edema**. *AJNR Am J Neuroradiol* 2003;24:254–256
2. Opeskin K, Silberstein M. **False-positive diagnosis of subarachnoid haemorrhage on computed tomography scan.** *J Clin Neurosci* 1998; 5:382–386

Standardized Calculation of Brain Parenchymal Fraction: An Approach to Objective Assessment of Cerebral Atrophy

Various approaches to measure brain atrophy in MR imaging have been applied until now, including measures of ven-

tricular width and volume estimates of the whole brain or of limited regions of interest. Recently, Ge et al (1) proposed a semiautomated segmentation algorithm calculating fractional gray matter (GM) and white matter (WM) volumes from volumetric MR imaging data sets that were normalized to total intracranial volume.

Ge et al demonstrated a marked age dependency of GM and WM fractional volumes. If one combines the values of fractional GM and WM volumes into the ratio of brain parenchymal volume to total intracranial volume, the resulting measure is the brain parenchymal fraction (BPF). This measure, first introduced by Rudick et al (2), has been validated as a useful quantitative MR imaging marker for investigating destructive processes ongoing in relapsing-remitting multiple sclerosis and has been applied for intraindividual longitudinal monitoring (eg, in controlled therapy trials [3]).

Such standardized measures, however, have yet to enter into general clinical practice. Although many of previous approaches for quantifying brain atrophy suffered from major drawbacks—availability of (costly) software, reproducibility of measures, and comparability with previously published results—standardized protocols offer a possible solution for quantitative assessment of atrophy instead of visual inspection alone. BPF may also be calculated in a highly automated and observer-independent way by using the algorithms implemented in Statistical Parametric Mapping software (4; SPM2b, Wellcome Department of Cognitive Neurology, London, [http://www.fil.ion.ucl.ac.uk/spm/spm2b.html]). Because SPM, in all its versions from 1994 until 2002, is freely available to the scientific public and has meanwhile gained a general acceptance for application to clinical studies, there now exists a fast, widely available, and validated method to generate an accurate measure of global brain atrophy in terms of BPF values that may be included in every single report of an individual MR imaging scan in routine diagnostics for neurodegenerative disease.

Discriminating between shrinkage of the brain considered to be appropriate for the patients' age and atrophy because of neurodegenerative disease may thus turn from an inherently subjective diagnosis to a rational diagnosis based on an objectively quantified measure. Prerequisite, however, for correct interpretation of BPF values from a single patient is the presence of BPF values from an age- and sex-matched normal database, as age and sex effects have been demonstrated previously (1, 5). Because of its standardized calculation, BPF values from normal controls can easily be shared with the neuroimaging community.

Freimut D. Juengling
Department of Radiology, Neuroradiology and Nuclear Medicine
Inselspital and University Hospital of Bern
Bern, Switzerland
Jan Kassubek
Department of Neurology
University of Ulm
Ulm, Germany

References

1. Ge Y, Grossman RI, Babb JS, et al. **Age-related total gray matter and white matter changes in normal adult brain. Part I. Volumetric MR imaging analysis.** *AJNR Am J Neuroradiol* 2002;23:1327–1333
2. Rudick RA, Fisher E, Lee JC, et al. **Brain atrophy in relapsing multiple sclerosis: relationship to relapses, EDSS, and treatment with interferon beta-1a.** *Mult Scler* 2000;6:365–372
3. Fisher E, Rudick RA, Cutter G, et al. **Relationship between brain atrophy and disability: an 8-year follow-up study of multiple sclerosis patients.** *Mult Scler* 2000;6:373–377
4. Chard DT, Parker GJ, Griffin CM, et al. **The reproducibility and sensitivity of brain tissue volume measurements derived from an SPM-based segmentation methodology.** *J Magn Reson Imaging* 2002; 15:259–267
5. Chard DT, Griffin CM, Parker GJ, et al. **Brain atrophy in clinically early relapsing-remitting multiple sclerosis.** *Brain* 2002;125:327–337

Reply:

I don't have much more comments on this letter except one thing mentioned in the letter. The brain parenchymal fraction was not first introduced by Rudick et al. This was first introduced by Micheal D. Phillips et al. in the article: Comparison of T2 lesion volume and magnetization transfer ratio histogram analysis and of atrophy and measures of lesion burden in patients with multiple sclerosis. AJNR 1998;19:1055–1060. In that article they called it as "percentage of brain parenchyma."

Yulin Ge
Department of Radiology
New York University
New York, NY

Erratum

In the article **Curved-Surface Projection: An Alternative Method for Visualizing Functional MR Imaging Results** by Scheef L et al. AJNR 24: 1045–1048, June/July 2003, the authors would like to acknowledge a mistake in the list of authors as printed. The author list which reads as follows: Lukas Scheef, Klaus Hoenig, Horst Urbach, Hans Schild and Roy Koenig is corrected as **Lukas Scheef, Klaus Hoenig, Horst Urbach, Christiane Kuhl, Hans Schild, and Roy Koenig**.